Determination of Kinetics of CO_2 Absorption in Solutions of 2-Amino-2-Methyl-1-Propanol Using a Microfluidic Technique

Chen Zheng, Bochao Zhao, Kai Wang, and Guangsheng Luo
The State Key Lab of Chemical Engineering, Dept. of Chemical Engineering, Tsinghua University, Beijing 100084, China

DOI 10.1002/aic.14972
Published online August 22, 2015 in Wiley Online Library (wileyonlinelibrary.com)

The kinetics for the reactions of carbon dioxide with 2-amine-2-methyl-1-propanol (AMP) and carbon dioxide (CO_2) in both aqueous and nonaqueous solutions were measured using a microfluidic method at a temperature range of 298–318 K. The mixtures of AMP-water and AMP-ethylene glycol were applied for the working systems. Gas-liquid bubbly microflows were formed through a microsieve device and used to determine the reaction characteristics by online observation of the volume change of microbubbles at the initial flow stage. In this condition, a mathematical model according to zwitterion mechanism has been developed to predict the reaction kinetics. The predicted kinetics of CO_2 absorption in the AMP aqueous solution verified the reliability of the method by comparing with literatures' results. Furthermore, the reaction rate parameters for the reaction of CO_2 with AMP in both solutions were determined. © 2015 American Institute of Chemical Engineers *AIChE J*, 61: 4358–4366, 2015
Keywords: kinetics, CO_2 absorption, microfluidic device, nonaqueous solution

Introduction

It is acknowledged that carbon dioxide (CO_2) accounts for the most amount (77%) of greenhouse gases emitted to the atmosphere.[1] Chemical absorption is generally considered as a reliable technology for CO_2 capture from power plant by post-combustion process.[2] The energy consumption is the major concerning in chemical absorption processes. Many researchers have studied the CO_2 absorption performance of several kinds of alkanolamines.[3–6] 2-Amine-2-methyl-1-propanol (AMP) as a sterically hindered amine has been proved to be an ideal amine for CO_2 absorption for its lower energy consumption for regeneration.[7] Meanwhile, the way of replacing water with low volatility chemicals as solvents has been suggested for reducing the energy consumption further.[8–11] For nonaqueous AMP solutions, the lower heat capacity of solutions, the reduced evaporation of the absorbents combined with the lower stripping temperature, all together should reduce the energy requirement.[10] The gas-liquid equilibrium data of CO_2 in AMP aqueous and AMP nonaqueous solutions have been published in many studies.[4,8,9,11] The reaction kinetics of CO_2 in the AMP aqueous solution has also been studied. Sartori et al.[12] reported the reaction kinetics of CO_2 absorption into the AMP aqueous solution; Yih and Shen[13] reported a rate constant of 1270 m^3/kmol/s at 313 K; Xiao et al.[3] reported overall pseudo-first-order reaction rate constants (k_{ov}) from 303 to 313 K; Choi et al.[14] reported k_{ov} from 293 to 323 K. However, there are few papers studying on kinetics of CO_2 in AMP nonaqueous. For AMP nonaqueous solutions, such as AMP-glycol solution, as viscosity of the solvent is relatively higher, it is more difficult to obtain the accuracy kinetics. The improvement of measuring technique and the study on the kinetics of the new absorption system are highly required for better understanding and design of CO_2 absorption processes.

Microfluidic technique has been widely used for intensification of many chemical processes, due to its high mass-transfer efficiency, safety, repeatability, and controllability. Tan et al.[15] have used a gas-liquid microdispersion device to measure the intrinsic reaction kinetics constant of oxidation of hydrogenated 2-ethyltetrahydroanthraquinone. An online visualization method has been successfully developed in some previous works to obtain the overall mass-transfer rate for gas-liquid segmented flow in a microfluidic device.[16,17] The mass-transfer coefficient for CO_2-water system in microchannel was reported as $1–3 \times 10^{-4}$ m/s. The mass-transfer characteristics of bubbly flow in T-junction microchannel was also studied.[18] It was found that microfluidic technique was efficient in mass transfer as well as mixing. Wang et al. used microsieve dispersion device to realize mass production of emulsions.[19] We also studied the generation rules of bubbles for gas-liquid system in microsieve dispersion device,[20] monodispersed bubbles could be prepared at relatively high gas-liquid ratio.

On the basis of previous work, we have developed a microfluidic method for the measurement of gas-liquid heterogeneous reaction kinetics and introduced this method to measure the kinetics of CO_2 absorption in the AMP-water and AMP-ethylene glycol (EG) solutions, respectively. The obtained kinetics data of CO_2-AMP-water system was used to verify the reliability of this new measurement technique by comparing with literature's results. Then, the reaction kinetics of CO_2 with AMP in EG solvent was determined, and a mathematical model has been developed. This work may provide valuable

Correspondence concerning this article should be addressed to G. Luo at gsluo@tsinghua.edu.cn.

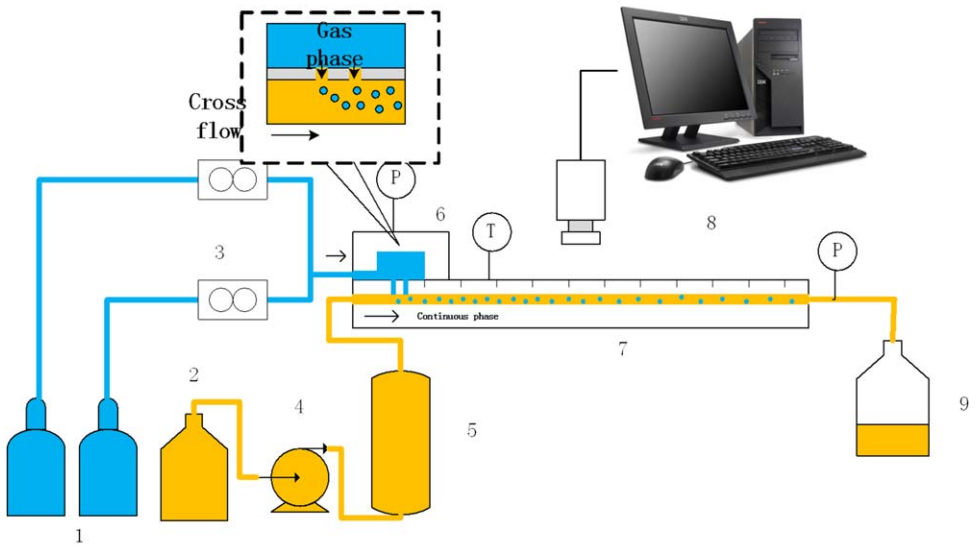

Figure 1. Experimental setup.

[Color figure can be viewed in the online issue, which is available at wileyonlinelibrary.com.]

information for design and optimization of CO_2 absorption processes with AMP solutions. It could also provide a reference for the study of gas-liquid heterogeneous reaction kinetics using microfluidic devices.

Experimental Section

Experimental setup

As shown in Figure 1, the experimental setup consists of three parts: transportation, microcontactor, and observation part. N_2 and CO_2 were delivered through mass flow meters with a measurement accuracy of $\pm 1.0\%$ independently. Two gaseous flows mixed in a 2-m long tube with an inner diameter of 2 mm. The liquid phase was transported in an indirect way, as the viscosity of AMP-EG solution is relatively high. The solution was stored in a piston buffer tank. An advection pump with a measurement accuracy of $\pm 1.0\%$ was used to pump water into the tank to push the piston. Then, the piston pushed the solution into the contactor. Before the experiment, we would make sure that no air existed in the tank. The gas phase was dispersed into the liquid phase in a microcontactor with a dispersion medium of two-sieve chip. The sieves both with a diameter of 0.30 mm were arranged in a radial-array. The chip was sealed with other two plates by a thermocompressor following the instruction of our previous work.[20] All parts of microcontactor were made of polymethyl methacrylate. The intersecting channel sculptured on the plate under the sieve-chip was 0.6 mm deep and 2.0 mm wide. An observation channel attached directly downstream to intersecting channel was 1.5 mm deep, 2.0 mm wide, and 100 mm long. Calibrations were engraved on the observation channel evenly with an interval of 10 mm. We used a microscope attached with a CCD camera to trace the diameter of bubbles along both intersecting and observation channel. A pressure gage with a measurement accuracy of $\pm 1\%$ was installed at the entrance of device to measure the pressure drop through the microdevice. Two thermometers with a measurement accuracy of ± 0.1°C were also installed at the entrance of contactor and the exit of observation room to measure the difference of temperature during the absorption process. In this work, we measured a pressure drop less than 5 kPa. We also measured the difference of temperature within 1.0°C. We introduced the continuous phase into the channels for 2 h before the experiment considering the wetting property of channel walls. The flow was maintained for 3 min before measurement, then we moved the scope from upstream to downstream of the channel to get the overall absorption rate.

Materials

We used AMP aqueous or AMP-EG solutions as the continuous phase. EG with analytically pure was purchased from Beijing Modern Oriental Fine Chemistry Co. AMP with a concentration of 97% was purchased from Shanghai Aladin. We used mixture gas of N_2 and CO_2 as the dispersed phase. N_2 with a purity of 99.995 mol % and CO_2 with a purity of 99.995 mol % were both purchased from Beijing Huayuan Gas Chemical Industry Co.

Operation and observation

A microscope (BXFM, Olympus) attached with a high-speed CMOS camera (DK-2740, Dantec Dynamics) was used to trace the bubble-flowing stage with frame frequencies of 2000 fps. The gas flow rate (Q_g) changed from 20 to 60 mL/min, while the liquid flow rates (Q_l) was maintained at 30 mL/min. The superficial velocity of liquid phase through the intersecting channel was 0.42 m/s. The average residence time of gas-liquid fluid in observation channel was 0.40 s. As the time of bubble formation was less than 1 ms, we only considered the residence time during the bubble-flowing stage. In our experiments, the polydispersity index for microbubbles was less than 3%, indicating that the microbubbles were highly uniform.

Table 1. Viscosities of AMP-EG Solutions and CO_2 Diffusivities

[AMP] (mol/L)	0	0.5	1.0	1.5	2.0
Viscosity (mPa s)	17.0	18.5	20.8	23.1	25.4
10^9 D_{CO_2} (m^2 s)	0.301	0.280	0.253	0.235	0.218

Physical properties

Physical properties of the solutions: viscosity, density, Henry's constant, and diffusivity of CO_2 are necessary to determine the parameters of mass transfer and reaction. For the AMP-water solution, Henry's law constant of CO_2 has been presented in many literatures using the N_2O analogy, Choi[14] presented a polynomial function involving the temperature and solvent concentration, as shown in Eq. 1. We could use this equation to predict the Henry's law constant (kPa m^3/kmol)

$$H_{CO_2} = (1.2288 + 5.2740 \times 10^{-2}[\mathrm{AMP}]) \exp\left(\frac{-1.6750 \times 10^3}{T}\right) \times 10^6 \quad (1)$$

We used a function derived by Choi to predict the diffusivities of CO_2 in the AMP aqueous solution, as shown in Eq. 2. The AAD% between calculated H and experimental H is below 1.23%, while the AAD% of D is below 4.26%, according to the Choi's work

$$D_{CO_2} = (1.2376 \times 10^3 - 1.6624 \times 10^2[\mathrm{AMP}] + 1.0966 \times 10[\mathrm{AMP}]^2) \exp\left(\frac{-2.0033 \times 10^3}{T}\right) \times 10^{-9} \quad (2)$$

For the AMP-EG solution, we measured the Henry's law constant of CO_2 in EG solution at 298 K in our previous work,[9] which is 2402 kPa m^3/kmol. The result also fitted the results presented in other literatures well.[21] Diffusivity of CO_2 in EG solution at 298 K was estimated with the aid of literature data and a semiempirical Stokes–Einstein relation. Oyevaar et al. derived a modified Stokes–Einstein relation as shown in Eq. 3[22]

$$(D_{CO_2}\mu_L^{0.8})_{amine soln} = \text{constant} = (D_{CO_2}\mu_L^{0.8})_{pure solvent} \quad (3)$$

The viscosities of AMP-EG solutions were measured by a viscometer (LVDV-II+Pro) made by Brookfield Engineering Laboratories. It is suggested that this relation can be used in the liquid phase with a viscosity from 1.0 up to 40 mPa s. Accordingly, we can estimate the diffusivities of CO_2 in AMP-EG solutions (Table 1).

Determination of reaction kinetics

In this work, the change of bubble volume at the initial flow stage was recorded directly by an online measurement method. Then, these data were analyzed to determine the overall mass-transfer rate and reaction kinetics. Before the analysis, we should assume that:

1. The mixture gas of CO_2-N_2 could be regarded as ideal gas.
2. The amount of N_2 dissolved in solution could be ignored as N_2 is considered as an inert component.
3. The evaporation of liquid solutions could be ignored.
4. As the loading of CO_2 ranged from 0.01 to 0.04 mol CO_2/mol Amine, the physical properties of the liquid phase and concentration of amine remain unchanged.
5. As the pressure drop along the channel is less than 5 kPa and the additional pressure induced by interfacial tension is about 618 Pa, the effect of pressure on the bubble size could be ignored and the pressure in bubble remains constant, equal to the pressure of mixture fluid.

Typical images of absorption process in the observation channel are shown in Figure 2, from which we can see that the gas phase is dispersed in the form of discrete bubbles into the continuous liquid phase. The size of the spherical bubbles decreases gradually along the observation channel due to the absorption of CO_2. The bubble sizes are uniform, with a polydispersity index less than 3%.

Under assumption (2), we can know that reduction of gas-phase volume is equal to the reduction of CO_2. Based on the conservation principle and the ideal gas law, the mass-transfer rate of CO_2 for a single bubble can be expressed by following equation

$$\frac{dn_{CO_2}}{dt} = \frac{p}{RT}\frac{dV_b}{dt} \quad (4)$$

where n_{CO_2} is the amount of CO_2 in a single bubble (kmol). V_b calculated from the average bubble diameter d_b ($V_b = \frac{\pi d_b^3}{6}$) is the volume of a single bubble. When the gas-side mass-transfer resistance can be ignored, the mass-transfer rate can be expressed below

$$N_{CO_2} = \frac{dn_{CO_2}}{dt} = k_L A(c^i_{CO_2} - c^b_{CO_2}) \quad (5)$$

where k_L is the liquid film mass-transfer coefficient (m/s), $c^i_{CO_2}$ is the concentration at the interfacial area while $c^b_{CO_2}$ is

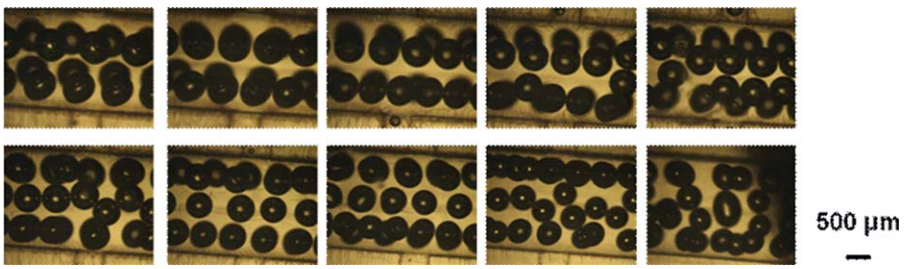

Figure 2. Typical images of absorption process in observation channel. (The pictures, ordered from the left to the right and the up to the down, represent the observation position from upstream to downstream; 1.0 kmol/m^3 AMP-EG, Q_g = 20 mL/min, Q_l = 30 mL/min).

[Color figure can be viewed in the online issue, which is available at wileyonlinelibrary.com.]

the concentration in the liquid bulk (kmol/m^3). A ($A=\pi d_b^2$) is the interfacial area, which varied as the change of bubble diameter (m^2). The concentration of the dissolved gas at the interface can be calculated using Henry's coefficient

$$c^{i}_{CO_2}=\frac{p_{CO_2}}{H_{CO_2}} \tag{6}$$

where p_{CO_2} is the partial pressure of CO_2.

The mass-transfer rate was enhanced by the addition of AMP, this enhancing effect can be explicated by enhancement factor E. In this way, the mass transfer can be expressed as below

$$N_{CO_2}=\frac{dn_{CO_2}}{dt}=Ek_L A(c^{i}_{CO_2}-c^{b}_{CO_2}) \tag{7}$$

Many expressions of enhancement factor have been derived based on a variety of theories such as two-film model, penetration, and surface renewal theory. In order to determine the enhancement factors of a reaction with mth order in relation to the gaseous reactant and nth order in relation to the liquid reactant, the Hatta number is applied

$$Ha=\frac{\sqrt{(2/(m+1))kc_i^{m-1}c_j^n D_i}}{k_L} \tag{8}$$

where k is the reaction rate constant of (m, n)th-order and D_i is the diffusion coefficient of the reacting gas (CO_2) in the liquid phase.

The chemical reactions during the absorption can be expressed by following equation

$$CO_2+RNH_2 \underset{k_{-1}}{\overset{k_2}{\rightleftarrows}} RNH_2^+COO^- \tag{I}$$

$$RNH_2^+COO^-+RNH_2 \xrightarrow{k_{amine}} RNHCOO^-+RNH_3^+ \tag{II}$$

$$RNH_2^+COO^-+H_2O \xrightarrow{k_{H_2O}} RNHCOO^-+H_3O^+ \tag{III}$$

$$RNH_2^+COO^-+OH^- \xrightarrow{k_{OH^-}} RNHCOO^-+H_2O \tag{IV}$$

The overall rate of reaction of CO_2 in amine aqueous solutions can be expressed as

$$r_{CO_2}=\frac{k_2[CO_2][RNH_2]}{1+k_{-1}/\sum k_b[B]}=k_{ov}[CO_2] \tag{9}$$

$$k_{ov}=\frac{[RNH_2]}{\frac{1}{k_2}+\frac{1}{\frac{k_2k_{H_2O}}{k_{-1}}[H_2O]+\frac{k_2k_{OH^-}}{k_{-1}}[OH^-]+\frac{k_2k_{amine}}{k_{-1}}[RNH_2]}} \tag{10}$$

k_{ov} is overall pseudo-first-order reaction rate constant. The slope of the straight line fitting the data of $\ln r_{CO_2}$ vs. $\ln p_{CO_2}$ will give the order of m with respect to the dissolved gas concentration. The order of n with respect to the amine concentration can also be determined. It was acknowledged that for the reaction between CO_2 and AMP, $m=1$, $n=1$. As a result, the Ha can be expressed as

$$Ha=\frac{\sqrt{k_{ov}D_{CO_2}}}{k_L} \tag{11}$$

For the first-order reaction, assuming that no gas exists in the liquid bulk, the following expressions of E have been found:

For the film model of mass transfer

$$E=\frac{Ha}{\tanh Ha} \tag{12}$$

For the penetration model of mass transfer

$$E=Ha\left[\left(1+\frac{\pi}{8Ha^2}\right)\mathrm{erf}\left(\sqrt{\frac{4Ha^2}{\pi}}\right)+\frac{1}{2Ha}\exp\left(-\frac{4Ha^2}{\pi}\right)\right] \tag{13}$$

For the surface renewal model of mass transfer

$$E=\sqrt{1+Ha^2} \tag{14}$$

In this work, k_{ov} for the reaction of CO_2 and AMP with a concentration of 1 mol/L was reported as 810 s^{-1},[23] k_L for CO_2-water system in microchannels was reported as 1–3 $\times$ 10^{-4} m/s.[16] The Ha can be calculated as 4.2–12.6, the enhancement factor can be assumed equal to the Hatta number ($E=Ha$) in all mass-transfer models. For AMP-EG system, the diffusivity of CO_2 is much lower than that in the aqueous solution. According to Fick's law, k_L is proportional to D_{CO_2}. As a result, the Ha for CO_2-AMP-EG system is higher than that for CO_2-AMP-H_2O system. The assumption for enhancement factor above is also satisfied.

For the fast chemical reaction between the dissolved gas CO_2 and AMP, the specific absorption rate is expressed as follows

$$N_{CO_2}=\frac{dn_{CO_2}}{dt}=\sqrt{D_{CO_2}k_{ov}}c^{i}_{CO_2} \tag{15}$$

To simplify the calculation, we introduced the residual rate of CO_2 (φ) to Eq. 4, as shown in Eq. 16

$$-\frac{dn_{CO_2}}{Adt}=-\frac{pV_{CO_2}}{ART}\frac{d\varphi}{dt} \tag{16}$$

where V_{CO_2} is the CO_2 volume in a single bubble. Other equations can be expressed below containing φ

$$c^{i}_{CO_2}=\frac{p_{CO_2}}{H_{CO_2}}=\frac{p(V_{CO_2}\cdot\varphi)}{H_{CO_2}V_b} \tag{17}$$

$$\sqrt{D_{CO_2}k_{ov}}=-\frac{H_{CO_2}V_b}{ART}\cdot\frac{d\ln\varphi}{dt}=-\frac{d_bH_{CO_2}V}{6RT}\cdot\frac{d\ln\varphi}{dt} \tag{18}$$

After dispersion process, during which gas-liquid bubbly flow was formed, the gas-liquid dispersion system flowed along the main channel. We measured over 100 bubbles at every observation position to get an average diameter of bubbles, the maximum relative standard deviation was less than 5%. The average bubble size ranged from 600 to 950 μm. It could be observed that the bubble diameter reduces as the flow distance increased, as CO_2 was absorbed into the solution. The initial dispersion sizes were nearly same at different temperature and amine concentration. When the absorption of CO_2 terminated, only N_2 remained in the bubble and thus the bubble size kept constant even the flowing distance increased further. Temperature might affect the terminal diameter of bubbles slightly, because higher temperature led to a larger bubble size according to ideal gas equation of state.

The heterogeneous mass-transfer amount of CO_2 could be determined by the reduction of the volume of bubble, V_g, which was calculated from the bubble diameter. Conversely, the residence time could be determined by flowing distance and the flow rate. Since the flow rate varied as the reduction of bubble volume, we used average flow rate between two detective positions to calculate the residence time, this method introduced a maximum deviation of 5% to the time.

Table 2. The Value of k_{ov} as a Function of AMP Concentration at Different Temperatures

T (K)	[AMP] (kmol/m^3)	k_{ov} (s^{-1})
300	1.0	731
300	1.5	1123
300	2.0	1477
308	1.0	954
308	1.5	1554
308	2.0	2272
318	1.0	1450
318	1.5	1954
318	2.0	3065

The value of residual rate of CO_2 is one initially, which reduces to zero as the residence time increases. Mass-transfer coefficients can be determined at different residence time. First, the data were fitted in polynomial with a R-square more than 0.993. Then, we could get the slope of a certain point and calculated the mass-transfer efficient using Eq. 18. k_{ov} could be also calculated through Eq. 15.

Results and Discussion

Reaction kinetics of CO_2 with AMP in the aqueous solution

We used mixture of CO_2 and N_2 as the dispersed phase, and the AMP aqueous solution as the continuous phase to study the reaction kinetics of CO_2 with AMP. We measured the absorption rate at 298, 308, and 318 K, with AMP concentrations of 1.0, 1.5, and 2.0 kmol/m^3. Choosing a lower concentration made the absorption process slower, as a result, the accuracy would increase. Using the data obtained at a lower concentration, we could set up a model to predict the performance at higher concentration. The CO_2 loading in this experiment was between 0.01 and 0.04. Keeping a low CO_2 loading would make sure that the physical properties of the liquid phase and concentration of amine remain unchanged. In this way, the measurement could be more accurate. The value of k_{ov} as a function of AMP concentration at different temperatures is shown in Table 2. k_{ov} increases with the increasing temperature and AMP concentration. Using these values of k_{ov}, we could calculate the residual rate of CO_2 at any given residence time, the comparisons between calculated results and experimental results are shown in Figure 3. These two results are in good agreement within the range of CO_2 partial pressure from 30 to 90 kPa. According to Figure 4a, the reaction is found to be first order with respect to both CO_2 and AMP. The second-order reaction rate constants (k_2) for AMP with CO_2 at different temperatures are also determined by each slope, suggested by Choi. The k_2 value of AMP at 298, 308, and 318 K was 746, 1080, and 1450 m^3/kmol/s, respectively, shown in Table 3. A comparison of k_2 within this work and some other works has been made, the result is shown in Figure 4b. Our value was similar to that measured through different methods. The little difference of the value was attributed to the different parameters (such as H_{CO_2} and D_{CO_2}).

The relation between k_2 and temperature is also shown in Figure 4b. A linear regression was used to relate the $\ln k_2$ and $1/T$, which led to the following equation

$$\ln k_2 = 17.20 - 3152/T \quad (19)$$

From the Arrhenius plot, we could calculate the activation energy of reaction between AMP and CO_2, which is 26.2 kJ/mol. This value is slightly higher than that of 25.1 kJ/mol obtained by Choi et al. and that of 24.261 kJ/mol obtained by Xu et al.[23] The result of kinetics of CO_2 absorption in the AMP aqueous solution could verify the reliability of this measurement method.

Reaction kinetics of CO_2 with AMP in EG solution

We measured the absorption rate at 298 K, with AMP concentrations of 0.5, 1.0, 1.5, and 2.0 kmol/m^3. When CO_2 was

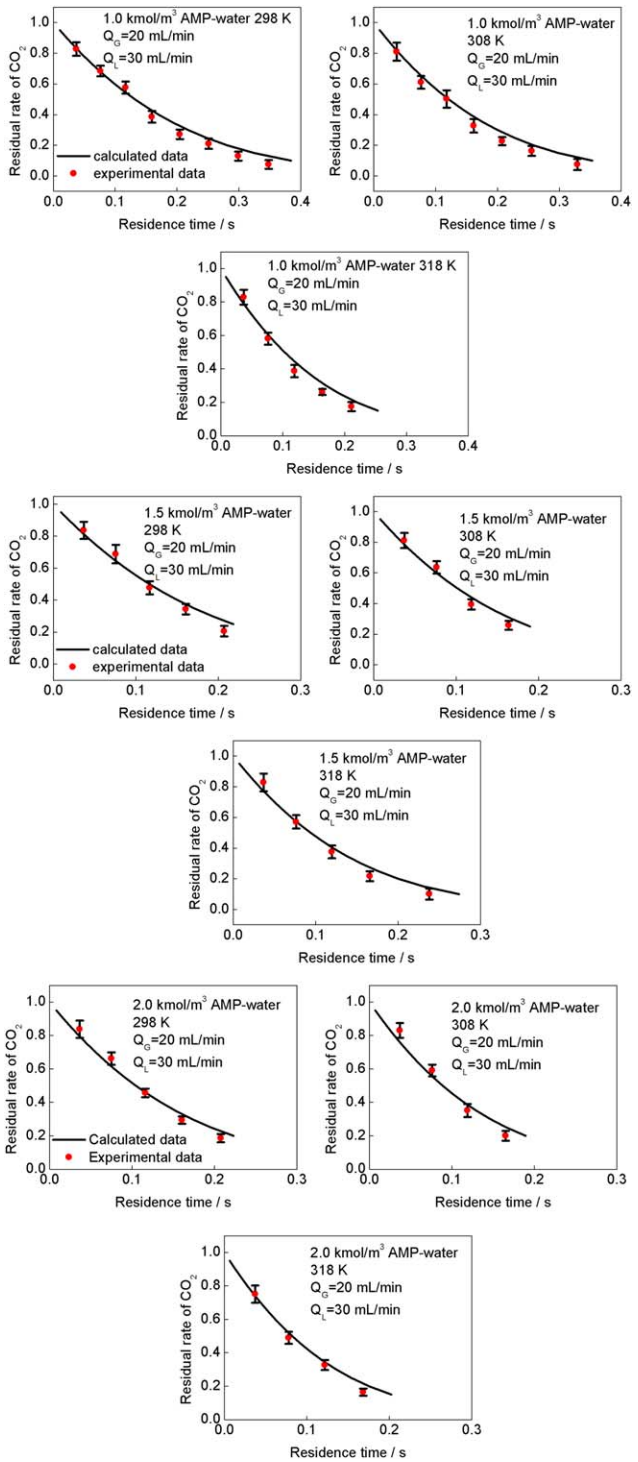

Figure 3. Comparisons between calculated results and experimental results for CO_2 absorption in aqueous AMP solutions.

[Color figure can be viewed in the online issue, which is available at wileyonlinelibrary.com.]

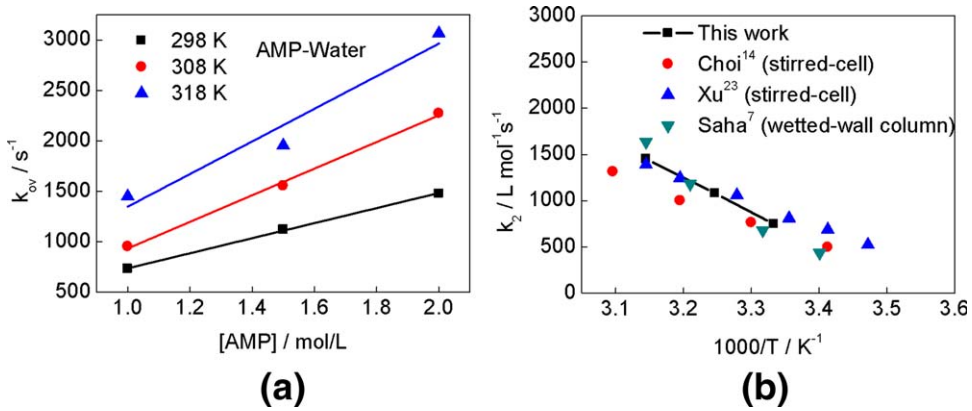

Figure 4. (a) The k_{ov} for AMP with CO_2 at different temperatures and AMP concentrations. (b) The second-order reaction rate constants (k_2) for AMP with CO_2 at different temperatures.

[Color figure can be viewed in the online issue, which is available at wileyonlinelibrary.com.]

absorbed in AMP-EG solution, no precipitation was seen up to a concentration of 3 mol/L (27% wt). In practical applications, we could increase the concentration of AMP further. A comparison between kinetics of CO_2 absorption in the AMP-H_2O and AMP-EG solutions is made, as shown in Figure 5. The CO_2 absorption rate in AMP-EG is lower than that in the AMP-H_2O system at the same temperature and concentration, due to the lower diffusivity of CO_2 in EG.

Figure 6 shows the effects of the initial CO_2 concentration and the gas flow rate on the mass-transfer coefficient. The mass-transfer coefficient changes slightly as the concentration of CO_2 changes. It also shows little change of mass-transfer coefficient with variation in the gas flow rate, as well as the bubble size, as shown in Figure 7, indicating that the gas-side resistance had little influence on overall mass transfer, especially at higher concentrations. As the continuous phase is split up into scattered parts by crowded bubbles, liquid-side mass transfer is enhanced significantly. The movement of bubbles also leads to the turbulence of continuous phase, which enhances the liquid-side mass transfer. When the bubbles were dispersed into liquid phase initially, the concentration of CO_2 was higher, as a result, the mass-transfer rate in liquid-film was higher. The concentration of the dissolved gas at the interface can be calculated using Henry's coefficient. As the CO_2 was absorbed, the mass-transfer rate in liquid-film decreased, the resistance in liquid-side had influence on the concentration of the dissolved gas at the interface. As the CO_2 at interface transferred in liquid slowly, the actual concentration of CO_2 at interface was higher than that calculated by Henry's coefficient. So that k_L calculated through Eqs. 5 and 6 at lower residual rate of CO_2 was higher due to the mass-transfer resistance in liquid-side, as shown in Figure 8. We chose the data from the initial measurement points (residual rate of $CO_2 > 0.70$) to calculate the mass-transfer coefficient k_L.

Table 3. The Second-Order Reaction Rate Constants (k_2) for AMP with CO_2 at Different Temperatures

T (K)	k_2 (m^3/kmol/s)
298	746
308	1080
318	1450

The kinetic data obtained at 298 K are listed in Table 4. Using these values of k_{ov}, we could calculate the residual rate of CO_2 at any given residence time, the comparisons between calculated results and experimental results are shown in Figure 9. These two results are in good agreement within the range of CO_2 partial pressure from 20 to 90 kPa. k_{ov} increases with the increase of AMP concentration, the slope of ln k_{ov} vs. ln [AMP] plot in figure gives a reaction order for AMP of 1.03, which indicates the formation of carbamate by a zwitterion mechanism. For nonaqueous solution AMP-EG, there was no exist of OH^-, so that EG and AMP molecules were mainly involved in process of deprotonation, suggested in our previous work.[8] The chemical reactions during the absorption can be expressed by following equation

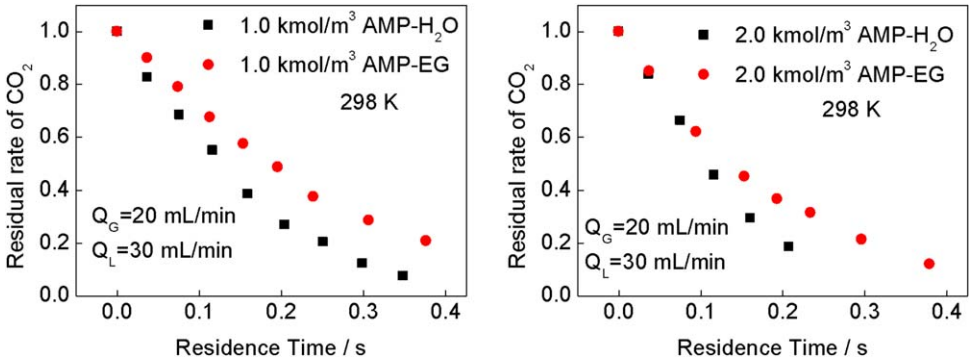

Figure 5. Comparison of kinetics of CO_2 absorption in different solutions.

[Color figure can be viewed in the online issue, which is available at wileyonlinelibrary.com.]

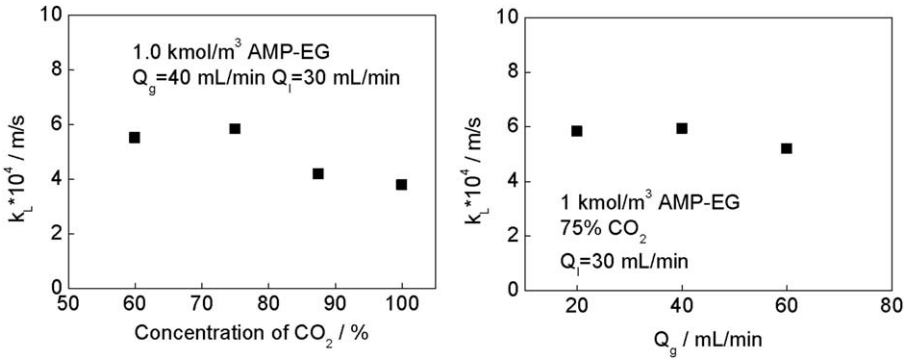

Figure 6. Effects of CO_2 concentration and Q_g on mass transfer.

$$CO_2 + RNH_2 \underset{k_{-1}}{\overset{k_2}{\rightleftharpoons}} RNH_2^+COO^- \quad \text{(V)}$$

$$RNH_2^+COO^- + EG \xrightarrow{k_{EG}} RNHCOO^- + EGH^+ \quad \text{(VI)}$$

$$RNH_2^+COO^- + RNH_2 \xrightarrow{k_{amine}} RNHCOO^- + RNH_3^+ \quad \text{(VII)}$$

The overall reaction rate of CO_2 in AMP-EG solution can be expressed as

$$k_{ov} = \frac{[AMP]}{\frac{1}{k_2} + \frac{1}{\frac{k_2 k_{EG}}{k_{-1}}[EG] + \frac{k_2 k_{AMP}}{k_{-1}}[AMP]}} \quad (20)$$

The second-order reaction rate constants (k_2) for AMP with CO_2 at in EG solvent is determined by the slope in Figure 10, which is 1075 s^{-1} at 298 K. This value is slightly higher than that of k_2 for AMP with CO_2 in aqueous solution (746 s^{-1} at 298 K). The values of factors ($D^{0.5}/H$) are responsible for the difference. The kinetics of AMP with CO_2 in nonaqueous solvent 1-propanol was studied by Xu et al.[23] They found that the slope of $\ln k_{app}$ vs. [AMP] gives a reaction order for AMP of 1.28, consistent with the formation of carbamate by zwitterions mechanism. However, a white carbamate precipitate could be observed during the reaction process in 1-propanol solvent, when the loading of CO_2 and the concentration of AMP were high, which could be easily dissolved into water or EG and could not be seen. The low stability of zwitterion in 1-propanol solvent resulted in a relatively high value for k_{-1}. k_2 was influenced by the solvent significantly, as k_2 for AMP with CO_2 in 1-propanol was just 56.3 m^3/kmol/s at 298 K, which was 810.4 m^3/kmol/s at 298 K in water presented in the same work by Xu and 1075 m^3/kmol/s at 298 K in EG presented in this work. The uncertainties in estimating solubility and diffusivity of CO_2 in AMP-EG solution may have influence on the value of k_2.

Conclusions

The reaction kinetics of CO_2 with AMP in the aqueous solution was studied using a microfluidic method at a temperature range of 298–318 K. The solutions concentration varied from 1 to 2 kmol/m^3. The well established zwitterions mechanism was used to explain the experimental results. The k_2 value of AMP at 300, 308, and 318 K was 746, 1080, and 1450 m^3/kmol/s, respectively, the results of k_2 was compared well with the literature data, which were obtained mostly from gas absorption studies using different methods such as stirred-cell, wetted-wall column. These data were in good agreement. From the Arrhenius regression of k_2, we could calculate the activation energy of reaction between AMP and CO_2, which was 26.2 kJ/mol. This value was higher than that of 25.1 kJ/mol obtained by Choi et al. and that of 24.261 kJ/mol obtained

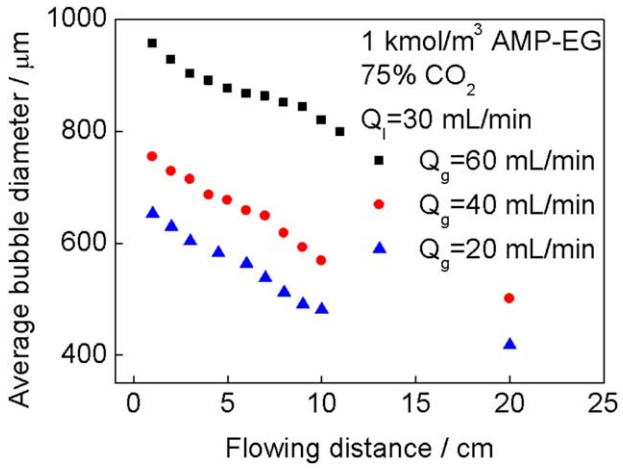

Figure 7. Effect of Q_g on the bubble size.

[Color figure can be viewed in the online issue, which is available at wileyonlinelibrary.com.]

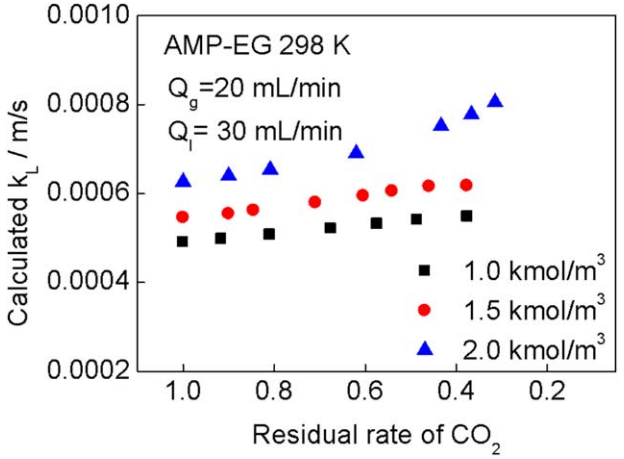

Figure 8. Effect of residual rate of CO_2 on k_L calculated by Eqs. 5 and 6.

[Color figure can be viewed in the online issue, which is available at wileyonlinelibrary.com.]

Table 4. The Kinetic Data for CO_2 into AMP-EG Solution at 298 K

[AMP] (kmol/m^3)	k_{ov} (s^{-1})
0.5	447
1.0	1041
1.5	1462
2.0	2098

by Xu et al., respectively. The result of kinetics of CO_2 absorption in aqueous AMP solution could verify the reliability of this measurement method. This work presents a direct and accurate way to measure the kinetics of gas-liquid system with chemical reaction.

The reaction kinetics for CO_2 with AMP in the EG solution was also studied using the same method at the temperature of 298 K. The solutions concentration varied from 0.5 to 2.0 kmol/m^3. It was found that CO_2 reacted with the AMP directly to form a zwitterion intermediate. For the nonaqueous system of AMP-EG, EG and AMP molecules react with zwitterion to produce a carbamate ion and a protonated base, leading eventually to carbamate ion. The overall absorption rate of CO_2 in aqueous AMP solution was much higher than that in AMP-EG solution. However, k_2 of AMP in water solvent was slightly lower than that in EG solvent. EG as solvent has little influence on reaction between CO_2 and AMP, but significant influence on mass transfer of CO_2 in solvent due to its higher viscosity. The lower absorption rate of CO_2 in nonaqueous AMP-EG solution will lead to a larger size of equipment. Conversely, using nonaqueous AMP solution as CO_2 absorbent can reduce the energy consumption of absorbent regeneration. There is a trade-off between capital costs and energy requirements. In our previous work,[24] we achieved a high mass-transfer efficiency of gas absorption into solution with high viscosity using a microfluidic device based on membrane contactor. With the development of high efficient absorption equipment for the relatively high viscosity system, both low energy consumption and low capital cost may be reached. This work can provide fundamental parameters of kinetics for further design and optimization of CO_2 capture process using nonaqueous AMP solution as absorbent. In our next work, we will consider mixture absorption systems such as aqueous AMP-piperazine (PZ) and any other nonaqueous AMP solutions. We can justify the use of AMP on its own by comparing the results of kinetic of CO_2 absorption in mixture solvent with that in sole AMP solution.

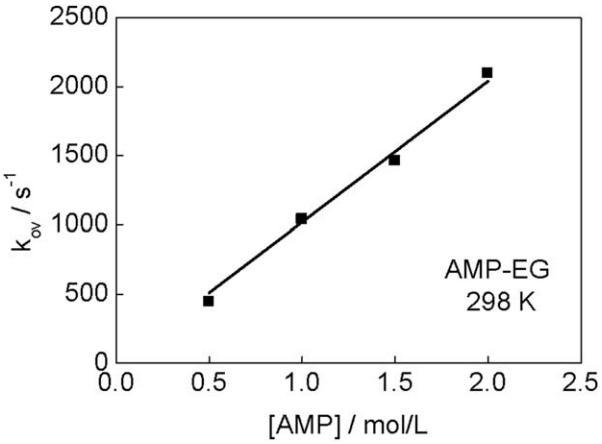

Figure 10. The k_{ov} for AMP with CO_2 at different temperatures and AMP concentrations.

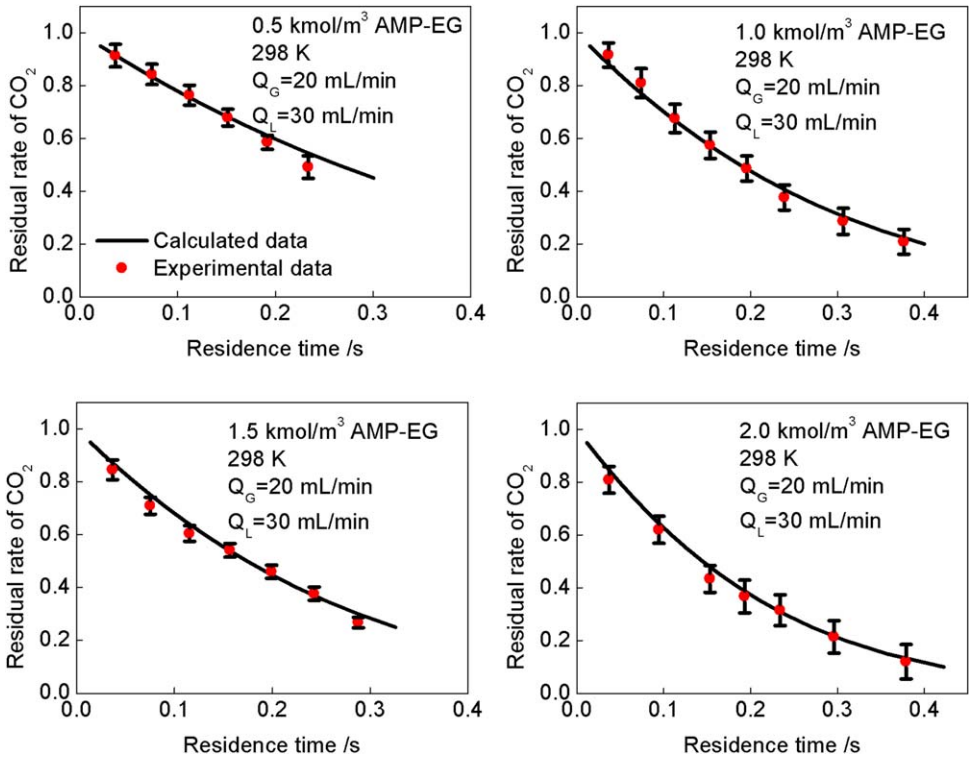

Figure 9. Comparisons between calculated results and experimental results for CO_2 absorption in AMP-EG solutions at 298 K.

[Color figure can be viewed in the online issue, which is available at wileyonlinelibrary.com.]

Acknowledgment

The authors would like to acknowledge the support of the National Natural Science Foundation of China (U1463208, 91334201).

Notation

H_{CO_2} = Henry law constant of CO_2, kPa m^3/kmol
D_{CO_2} = diffusivity of CO_2 in liquid, m^3/s
μ_L = viscosity of liquid, mPa s
n_{CO_2} = amount of CO_2 in a single bubble, kmol
d_b = average bubble diameter, m
V_b = volume of a single bubble, m^3
k_L = liquid film mass-transfer coefficient, m/s
$c^i_{CO_2}$ = concentration at the interfacial area, kmol/m^3
$c^b_{CO_2}$ = concentration in the liquid bulk, kmol/m^3
A = interfacial area, m^2
p_{CO_2} = partial pressure of CO_2, kPa
Ha = Hatta numer defined in Eq. 8
k_{ov} = overall pseudo-first-order reaction rate constant, s^{-1}
k_2 = second-order reaction rate constant in Eq. 9
k_b = second-order reaction rate constant for base B in Eq. 9
k_{-1} = rate constant for the reverse reaction in Eq. 9
k_{amine} = rate constant for deprotonation reaction in Eq. 10
k_{H_2O} = rate constant for deprotonation reaction in Eq. 10
k_{OH^-} = rate constant for deprotonation reaction in Eq. 10
k_{EG} = rate constant for deprotonation reaction in Eq. 20

Literature Cited

1. Yang HQ, Xu ZH, Fan MH, Gupta R, Slimane RB, Bland AE. Progress in carbon dioxide separation and capture: a review. *J Environ Sci*. 2008;20:14–27.
2. Oyenekan BA, Rochelle GT. Alternative stripper configurations for CO_2 capture by aqueous amines. *AIChE J*. 2007;53:3144–3154.
3. Xiao J, Li CW, Li MH. Kinetics of absorption of carbon dioxide into aqueous solutions of 2-amino-2-methyl-1-propanol + monoethanolamine. *Chem Eng Sci*. 2000;55:161–175.
4. Conway W, Bruggink S, Beyad Y, Luo WL, Melian-Cabrera I, Puxty G, Feron P. CO_2 absorption into aqueous amine blended solutions containing monoethanolamine (MEA), N,N-dimethylethanolamine (DMEA), N,N-diethylethanolamine (DEEA) and 2-amino-2-methyl-1-propanol (AMP) for post-combustion capture processes. *Chem Eng Sci*. 2015;126:446–454.
5. Monteiro JGMS, Hussain S, Majeed H, Mba EO, Hartono A, Knuutila H, Svendsen HF. Kinetics of CO_2 absorption by aqueous 3-(methylamino)propylamine solutions: experimental results and modeling. *AIChE J*. 2014;60:3792–3803.
6. Aboudheir A, Tontiwachwuthikul P, Chakma A, Idem R. Kinetics of the reactive absorption of carbon dioxide in high CO_2-loaded, concentrated aqueous monoethanolamine solutions. *Chem Eng Sci*. 2003;58:5195–5210.
7. Saha AK, Bandyopadhyay SS. Kinetics of absorption of CO_2 into aqueous solutions of 2-amino-2-methyl-1-propanol. *Chem Eng Sci*. 1995;50:3587–3598.
8. Zheng C, Tan J, Wang YJ, Luo GS. CO_2 solubility in a mixture absorption system of 2-amino-2-methyl-1-propanol with ethylene glycol. *Ind Eng Chem Res*. 2013;52:12247–12252.
9. Zheng C, Tan J, Wang YJ, Luo GS. CO_2 solubility in a mixture absorption system of 2-amino-2-methyl-1-propanol with glycol. *Ind Eng Chem Res*. 2012;51:11236–11244.
10. Barzagli F, Mani F, Peruzzini M. Efficient CO_2 absorption and low temperature desorption with non-aqueous solvents based on 2-amino-2-methyl-1-propanol (AMP). *Int J Greenhouse Gas Control*. 2013; 16:217–223.
11. Svensson H, Edfeldt J, Velasco VZ, Hulteberg C, Karlsson HT. Solubility of carbon dioxide in mixtures of 2-amino-2-methyl-1-propanol and organic solvents. *Int J Greenhouse Gas Control*. 2014; 27:247–254.
12. Sartori G, Ho WS, Savage DW, Chludzinski GR, Wiechert S. Sterically hindered amines for acid-gas absorption. *Sep Purif Methods*. 1987;16:171–200.
13. Yih SM, Shen KP. Kinetics of carbon dioxide reaction with sterically hindered 2-amino-2-methyl-l-propanol aqueous solutions. *Ind Eng Chem Res*. 1988;27:2237–2241.
14. Choi WJ, Min BM, Seo JB, Park SW, Oh KJ. Effect of ammonia on the absorption kinetics of carbon dioxide into aqueous 2-amino-2-methyl-1-propanol solutions. *Ind Eng Chem Res*. 2009;48:4022–4029.
15. Tan J, Du L, Lu YC, Xu JH, Luo GS. Development of a gas-liquid microstructured system for oxidation of hydrogenated 2-ethyltetrahydroanthraquinone. *Chem Eng J*. 2011;171:1406–1414.
16. Tan J, Lu YC, Xu JH, Luo GS. Mass transfer performance of gas-liquid segmented flow in microchannels. *Chem Eng J*. 2012;181–182:229–235.
17. Roudet M, Loubiere K, Gourdon C, Cabassud M. Hydrodynamic and mass transfer in inertial gas-liquid flow regimes through straight and meandering millimetric square channels. *Chem Eng Sci*. 2011; 66:2974–2990.
18. Yang L, Tan J, Wang K, Luo GS. Mass transfer characteristics of bubbly flow in microchannels. *Chem Eng Sci*. 2014;109:306–314.
19. Wang K, Lu YC, Xu JH, Luo GS. Droplet generation in micro-sieve dispersion device. *Microfluid Nanofluid*. 2011;10:1087–1095.
20. Zheng C, Zhao BC, Wang K, Luo GS. Bubble generation rules in microfluidic devices with micro-sieve array as dispersion medium. *AIChE J*. 2015;61:1663–1676.
21. Gui X, Tang ZG, Fei WY. Solubility of CO_2 in alcohols, glycols, ethers and ketones at high pressures from (288.15 to 318.15) K. *J Chem Eng Data*. 2011;56:2420–2429.
22. Oyevaar MH, Morssinkhof RWJ, Westerterp KR. Density, viscosity solubility and diffusivity of CO_2 and N_2O in solutions of diethanolamine in aqueous ethylene glycol at 298 K. *J Chem Eng Data*. 1989;34:77–82.
23. Xu S, Wang YW, Otto FD, Mather AE. Kinetics of the reaction of carbon dioxide with 2-amino-2-methyl-1-propanol solutions. *Chem Eng Sci*. 1996;51:841–850.
24. Tan J, Shao HW, Xu JH, Du L, Luo GS. Mixture absorption system of monoethanolamine−triethylene glycol for CO_2 capture. *Ind Eng Chem Res*. 2011;50:3966–3976.

Manuscript received Apr. 27, 2015, and revision received July 15, 2015.